European Journal of Nuclear Medicine and Molecular Imaging (2024) 51:443–454
https://doi.org/10.1007/s00259-023-06440-9

ORIGINAL ARTICLE

Distinct subtypes of spatial brain metabolism patterns in Alzheimer's disease identified by deep learning-based FDG PET clusters

Hyun Gee Ryoo[1,2,3] · Hongyoon Choi[2,4] · Kuangyu Shi[5] · Axel Rominger[5] · Dong Young Lee[6,7] · Dong Soo Lee[2,3,4] · for the Alzheimer's Disease Neuroimaging Initiative

Received: 24 May 2023 / Accepted: 8 September 2023 / Published online: 22 September 2023

Abstract

Purpose Alzheimer's disease (AD) is a heterogeneous disease that presents a broad spectrum of clinicopathologic profiles. To date, objective subtyping of AD independent of disease progression using brain imaging has been required. Our study aimed to extract representations of unique brain metabolism patterns different from disease progression to identify objective subtypes of AD.

Methods A total of 3620 FDG brain PET images with AD, mild cognitive impairment (MCI), and cognitively normal (CN) were obtained from the ADNI database from 1607 participants at enrollment and follow-up visits. A conditional variational autoencoder model was trained on FDG brain PET images of AD patients with the corresponding condition of AD severity score. The *k*-means algorithm was applied to generate clusters from the encoded representations. The trained deep learning-based cluster model was also transferred to FDG PET of MCI patients and predicted the prognosis of subtypes for conversion from MCI to AD. Spatial metabolism patterns, clinical and biological characteristics, and conversion rate from MCI to AD were compared across the subtypes.

Results Four distinct subtypes of spatial metabolism patterns in AD with different brain pathologies and clinical profiles were identified: (i) angular, (ii) occipital, (iii) orbitofrontal, and (iv) minimal hypometabolic patterns. The deep learning model was also successfully transferred for subtyping MCI, and significant differences in frequency ($P < 0.001$) and risk of conversion (log-rank $P < 0.0001$) from MCI to AD were observed across the subtypes, highest in S2 (35.7%) followed by S1 (23.4%).

Conclusion We identified distinct subtypes of AD with different clinicopathologic features. The deep learning-based approach to distinguish AD subtypes on FDG PET could have implications for predicting individual outcomes and provide a clue to understanding the heterogeneous pathophysiology of AD.

Keywords Alzheimer's disease · Mild cognitive impairment · Subtypes · FDG PET · Deep learning

Introduction

Alzheimer's disease (AD) is a heterogeneous disease that presents a broad spectrum of clinicopathologic profiles with variability in age of onset, clinical presentation, tau-related

Data used in preparation of this article were obtained from the Alzheimer's Disease Neuroimaging Initiative (ADNI) database (adni.loni.usc.edu). As such, the investigators within the ADNI contributed to the design and implementation of ADNI and/or provided data but did not participate in analysis or writing of this report. A complete listing of ADNI investigators can be found at http://adni.loni.usc.edu/wp-content/uploads/how_to_apply/ADNI_Acknowledgement_List.pdf.

✉ Hongyoon Choi
chy1000@snu.ac.kr

[1] Department of Nuclear Medicine, Seoul National University Bundang Hospital, Seongnam, Republic of Korea

[2] Department of Nuclear Medicine, Seoul National University Hospital, 101, Daehak-ro, Jongno-gu, Seoul 03080, Republic of Korea

[3] Department of Molecular Medicine and Biopharmaceutical Sciences, Graduate School of Convergence Science and Technology, and College of Medicine or College of Pharmacy, Seoul National University, Seoul, Republic of Korea

[4] Department of Nuclear Medicine, Seoul National University College of Medicine, Seoul, Republic of Korea

[5] Department of Nuclear Medicine, Inselspital, University of Bern, Freiburgstrasse 18, 3010 Bern, Switzerland

[6] Department of Neuropsychiatry, Seoul National University Hospital, Seoul, Republic of Korea

[7] Department of Psychiatry, Seoul National University College of Medicine, Seoul, Republic of Korea

pathology, and brain atrophy, despite common pathologic features, including amyloid and tau deposition [1–4]. Due to its heterogeneous biological pathology and clinical manifestations, there have been attempts to reveal biological subtypes of AD through structural magnetic resonance imaging (MRI) and tau positron emission tomography (PET) [5–7].

Since [^{18}F]fluorodeoxyglucose (FDG) PET represents neurological functions by neurometabolism coupling, it supports the differential diagnosis of neurodegenerative diseases [8, 9]. FDG PET has also been used to predict the progression of mild cognitive impairment (MCI) [10, 11]. Since FDG PET reflects spatial neuronal activity patterns in various diseases, it is more suitable than other images to match clinical symptom characteristics and image-based disease subtypes [12–14]. Recently, many attempts have been reported to differentiate spatial hypometabolic patterns of AD subtypes in a data-driven or hypothesis-driven manner [15–18]. However, a main concern of previous approaches in defining AD subtypes on various modalities has been the difficulty in differentiating the effect of disease progression [19]. The intrinsic biological subtype of AD differentiated from the disease severity has been a challenge since it should be achieved by patient data with various disease stages.

In this study, we utilized conditional variational autoencoder (cVAE) on FDG PET of AD subjects with the corresponding condition of AD severity score. VAE is an unsupervised deep learning method that learns representations to map data from latent space in a probabilistic manner [20]. Additionally, cVAE uses conditioned variables as auxiliary inputs to reflect hidden information other than given conditions [21]. Decreased FDG uptake patterns in the cortex mostly depend on disease severity, and it has been difficult to define subtypes by removing the effect of disease progression. Since a cVAE model directly uses conditional variables to generate images from latent features, latent features are expected to represent other data-specific features different from conditions, i.e., disease severity. In the current study, we aimed to identify AD subtypes using deep learning-based clustering on FDG PET images to understand the distinct spatial patterns of neurodegeneration. We also aimed to investigate the clinicopathologic features of subtypes defined by spatial brain metabolism patterns.

Materials and methods

Subjects

Data used in the preparation of this article were obtained from the Alzheimer's Disease Neuroimaging Initiative (ADNI) database. The ADNI was launched in 2003 to test whether serial MRI, PET, other biological markers, and clinical and neuropsychological assessment can be combined to measure the progression of MCI and early AD. We obtained 3620 FDG brain PET images from 1607 participants at enrollment (baseline) and follow-up visits between 2005 and 2020 from the ADNI database. Details regarding FDG PET data acquisition and preprocessing are available in the Supplementary Methods [22]. We defined groups of FDG PET images with AD, MCI, and cognitively normal (CN) based on the clinical diagnosis. Each repeated FDG PET scan of the same individual at different visits was independently assigned to the groups based on the clinical diagnosis at the time of the visit for the study. Based on the criteria, we included 838 FDG PET scans with AD, 1761 scans with MCI, and 1021 scans with CN for the present study. Written informed consent for cognitive testing and neuroimaging prior to participation was obtained from all subjects, and the study protocols were approved by the institutional review boards of all participating institutions.

Deep learning-based model for subtyping AD and MCI

We utilized cVAE to find hidden representations of FDG PET image patterns in AD. A total of 838 FDG brain PET images with AD were used as input images. The Clinical Demetria Rating Scale Sum of Boxes (CDR-SB) score was used as the corresponding condition vector of each image. CDR-SB is commonly used in clinical and research settings to stage dementia severity [23], so we chose CDR-SB as an input condition to remove the effect of disease severity of AD in latent features and find hidden representations. The CDR-SB score was rescaled to the range of 0 to 1, which was divided by a maximum CDR-SB score of 18 and used as input. The details of the cVAE architecture and training are summarized in Supplementary Methods (Supplementary Table 1 and Supplementary Fig. 1) [24]. To identify AD subtypes from the hidden representations on FDG PET image patterns, the *k*-means algorithm was applied to generate clusters from the encoded latent representations [25, 26]. The number of clusters was determined using the elbow method [27, 28]. Subsequently, the trained deep learning-based FDG PET cluster model in AD was directly transferred to the MCI images, without further training for subtyping MCI, to predict their subtypes and to identify differential trajectories and prognoses of subtypes in MCI. The details of the clustering method and model transfer are summarized in Fig. 1 and Supplementary Methods.

Clinical and biological characterization

We compared demographic, cognitive, and biomarker variables between clusters for the clinical and biological

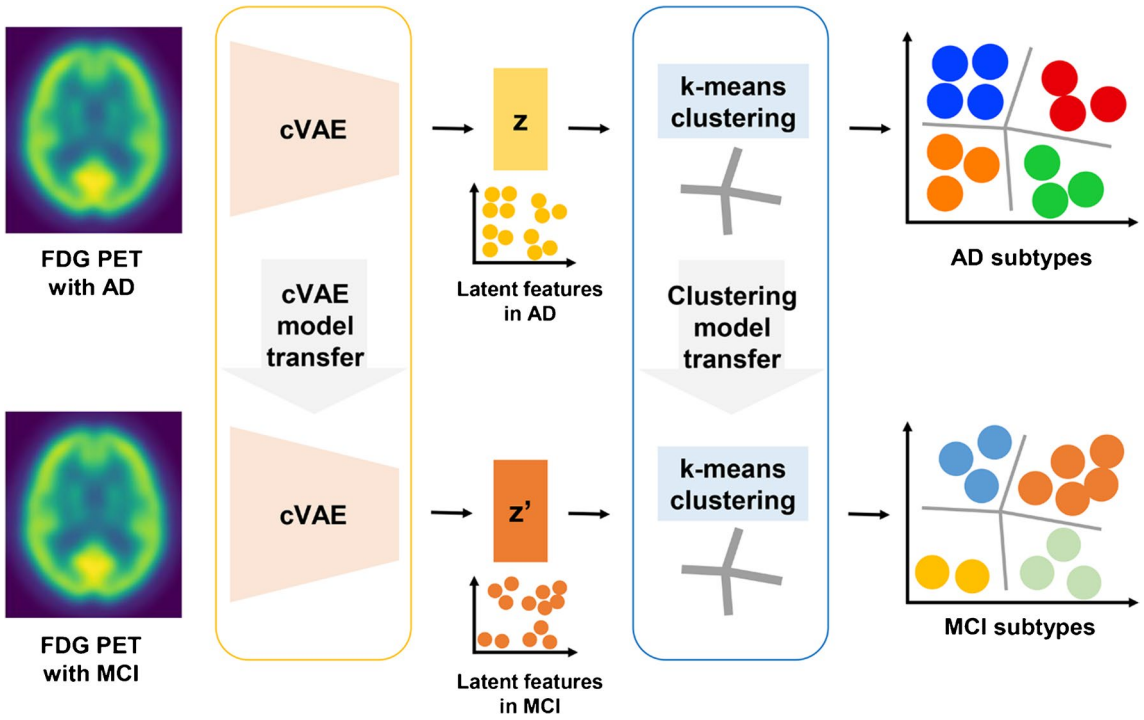

Fig. 1 Study design of the deep learning-based FDG PET cluster model for AD and MCI subtypes. The framework shows the clustering method for AD subtypes and the transfer of the deep learning model for MCI subtypes

characterization of subtypes. Characteristics of subtypes were compared in groups with all AD images regardless of repeated visits ($n = 838$); AD images only at the baseline visit without repeated scans from the same subject ($n = 292$); and all MCI images regardless of repeated visits ($n = 1761$). The demographic analyses compared age, sex, and years of education. The cognitive analyses compared CDR-SB, Mini-Mental State Examination (MMSE), Montreal Cognitive Assessment (MOCA) scores, and four cognitive domain scores. For the cognition domain scores, we used Alzheimer's Disease Sequencing Project Phenotype Harmonization Consortium composite cognitive scores: the harmonized composite memory score, executive function score, language score, and visuospatial score [29]. The biomarker variables for the comparison between clusters included APOE4 carriage, cerebrospinal fluid (CSF) amyloid-beta (Abeta), total tau (t-tau), phosphorylated tau (p-tau), and imaging biomarkers. The standardized uptake value ratio (SUVR) of [^{18}F]florbetapir (AV45) PET was the mean florbetapir uptake in the cortex of predefined volumes of interest, which was then divided by the activity of the whole cerebellum as a reference region. The amyloid positivity was defined as SUVR ≥ 1.11. The hippocampal volume to intracranial volume ratio (HV/ICV) measured on MRI was also calculated as an indicator of hippocampal atrophy.

Prognosis prediction of MCI subtypes

We defined as MCI converters those who converted from MCI to AD within 2 years from the baseline visit and as non-converters those who did not convert to AD during a follow-up of at least 2 years from the baseline visit. The time to conversion from MCI to AD was calculated for the subjects who had a change in diagnosis from MCI to AD at any time point. Kaplan-Meier survival curves were generated to evaluate the risk of conversion from MCI to AD across the subtypes.

Statistical analysis

Values are expressed as percentages or means with standard deviations (SDs). Group differences in demographic and clinical variables in subtypes were evaluated using one-way ANOVA with post hoc analysis and the chi-square test. The number of missing values in the analysis of each group is provided in the supplementary data. Averaged Z scores of demographic, cognitive, and biomarker variables of each subtype were used for heatmap generation. Kaplan-Meier survival analysis was used to test for subtype differences in conversion from MCI to AD, and curves were compared using the log-rank test. Statistical analyses were performed using Jamovi software (The jamovi project (2021). jamovi (Version 1.6). Retrieved from https://www.jamovi.org), and a P value less than 0.05 was considered statistically significant.

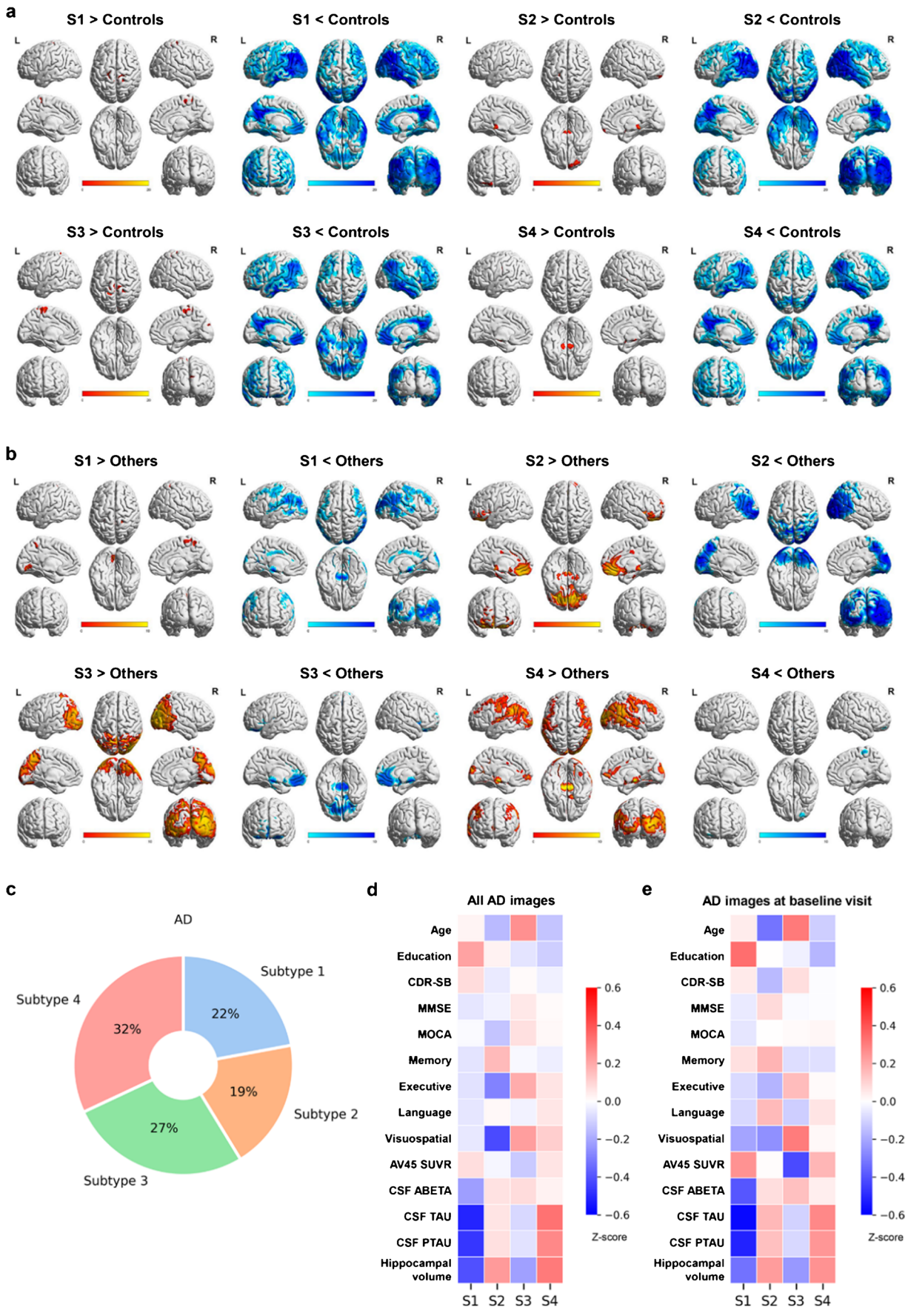
a
S1 > Controls
S1 < Controls
S2 > Controls
S2 < Controls
S3 > Controls
S3 < Controls
S4 > Controls
S4 < Controls
b
S1 > Others
S1 < Others
S2 > Others
S2 < Others
S3 > Others
S3 < Others
S4 > Others
S4 < Others
c
AD
Subtype 1
Subtype 2
Subtype 3
Subtype 4
22%
19%
27%
32%
d
All AD images
Age
Education
CDR-SB
MMSE
MOCA
Memory
Executive
Language
Visuospatial
AV45 SUVR
CSF ABETA
CSF TAU
CSF PTAU
Hippocampal volume
S1 S2 S3 S4
0.6
0.4
0.2
0.0
−0.2
−0.4
−0.6
Z-score
e
AD images at baseline visit
Age
Education
CDR-SB
MMSE
MOCA
Memory
Executive
Language
Visuospatial
AV45 SUVR
CSF ABETA
CSF TAU
CSF PTAU
Hippocampal volume
S1 S2 S3 S4
0.6
0.4
0.2
0.0
−0.2
−0.4
−0.6
Z-score

◂**Fig. 2** Distinct subtypes of spatial metabolism patterns in AD. Spatial metabolism patterns of AD subtypes compared with **a** cognitively normal controls and **b** all other subtypes. The colored bar indicates *t* values. **c** Frequency of AD subtypes. Heatmaps of clinical and biological characteristics of AD subtypes compared in groups with **d** all AD images and **e** AD images at the baseline visit

Results

Spatial brain metabolism pattern in AD subtypes

Of the 838 FDG brain PET images of patients with AD, four distinct AD subtypes were identified by deep learning-based FDG PET clusters. We set 4 as the subtype number since the inflection point appeared when the number was 4 on the elbow method plot (Supplementary Fig. 2).

Spatial brain metabolism patterns of AD subtypes on FDG PET with cerebellar normalization were compared with those of the CN. All AD subtypes shared a common pattern of hypometabolism involving the frontal, parietal, and temporal lobes, precuneus, and posterior cingulate cortex. In addition to typical AD patterns shared across all subtypes, subtype-specific regions of hypometabolism were observed in each subtype (Fig. 2a and Supplementary Fig. 3). Subtype 1 (S1: angular) included 185 (22%) AD patients and showed prominent hypometabolism in the angular gyrus with a diffuse hypometabolism pattern involving the parietotemporal, frontal, limbic, occipital, and cingulate cortices. Subtype 2 (S2: occipital) included 161 (19%) AD patients and showed prominent hypometabolism in the occipital cortex with a posterior-predominant hypometabolism pattern involving the occipital, posterior-parietal cortices, and precuneus. Subtype 3 (S3: orbitofrontal) included 224 (27%) AD patients and showed prominent hypometabolism in the orbitofrontal cortex with an anterior-predominant hypometabolism pattern involving the frontal, limbic, and anterior cingulate cortices. Subtype 4 (S4: minimal) included 268 (32%) AD patients and showed no additional hypometabolic region. Subtype-specific spatial metabolism patterns also corresponded to the regions observed in the comparisons between one subtype and all of the other subtypes (Fig. 2b). To exclude the effects of overlapping images from the same subject at different visits, spatial metabolism patterns of AD subtypes for the individuals only at the baseline visits were compared with CN controls using FDG PET images with cerebellar normalization. For the FDG PET with AD at the baseline visit, S1 (angular), S2 (occipital), S3 (orbitofrontal), and S4 (minimal) included 58 (20%), 52 (18%), 83 (28%), and 99

Table 1 Clinical and biological characteristics of AD subtypes

	CN	AD ($n = 838$)				*P* value, global comparison (S1, S1, S3, and S4)
		S1	S2	S3	S4	
Demographics						
n (%)	1021	185 (22%)	161 (19%)	224 (27%)	268 (32%)	
Age, years	75.7 (6.2)	76.4 (7.2)	75.0 (7.5)	78.2 (6.5)	75.2 (7.9)	< 0.001***
Sex, female (%)	43%	5%	32%	41%	72%	< 0.001***
Education, years	16.3 (2.8)	16.1 (3.3)	15.5 (2.6)	15.3 (2.7)	15.1 (2.9)	0.009**
Cognition						
CDR-SB	0.1 (0.4)	5.5 (2.7)	5.2 (2.7)	5.4 (2.6)	5.3 (2.3)	0.609
MMSE	29.0 (1.2)	21.9 (4.0)	22.0 (4.4)	22.3 (3.8)	22.2 (3.9)	0.699
MOCA	25.8 (2.5)	16.7 (4.9)	16.0 (5.2)	17.1 (4.8)	16.8 (5.0)	0.645
Memory score	0.86 (0.51)	−0.92 (0.49)	−0.81 (0.53)	−0.89 (0.46)	−0.90 (0.45)	0.217
Executive score	0.74 (0.48)	−0.55 (0.72)	−0.71 (0.74)	−0.36 (0.65)	−0.45 (0.70)	< 0.001***
Language score	0.80 (0.49)	−0.29 (0.59)	−0.24 (0.63)	−0.27 (0.62)	−0.22 (0.64)	0.630
Visuospatial score	0.10 (0.31)	−0.36 (0.61)	−0.60 (0.74)	−0.19 (0.52)	−0.26 (0.62)	< 0.001***
Biomarker						
AV45 SUVR	1.12 (0.19)	1.40 (0.24)	1.37 (0.22)	1.35 (0.25)	1.39 (0.21)	0.585
Amyloid positivity (%)	-	87%	89%	79%	88%	-
APOE4 carrier (%)	27%	68%	64%	68%	66%	0.249
CSF Abeta, pg/ml	1211 (439)	580 (276)	677 (402)	681 (345)	664 (280)	0.159
CSF t-tau, pg/ml	245 (91)	293 (108)	382 (158)	358 (124)	423 (173)	< 0.001***
CSF p-tau, pg/ml	23 (10)	29 (12)	38 (17)	35 (14)	41 (19)	< 0.001***
HV/ICV, cm^3/mm^3	4.78 (0.68)	3.37 (0.56)	3.80 (0.59)	3.50 (0.57)	3.85 (0.73)	< 0.001***

The data are expressed as percentages or means with standard deviations in parentheses. Missing values are excluded. *$P < 0.05$, **$P < 0.01$, ***$P < 0.001$

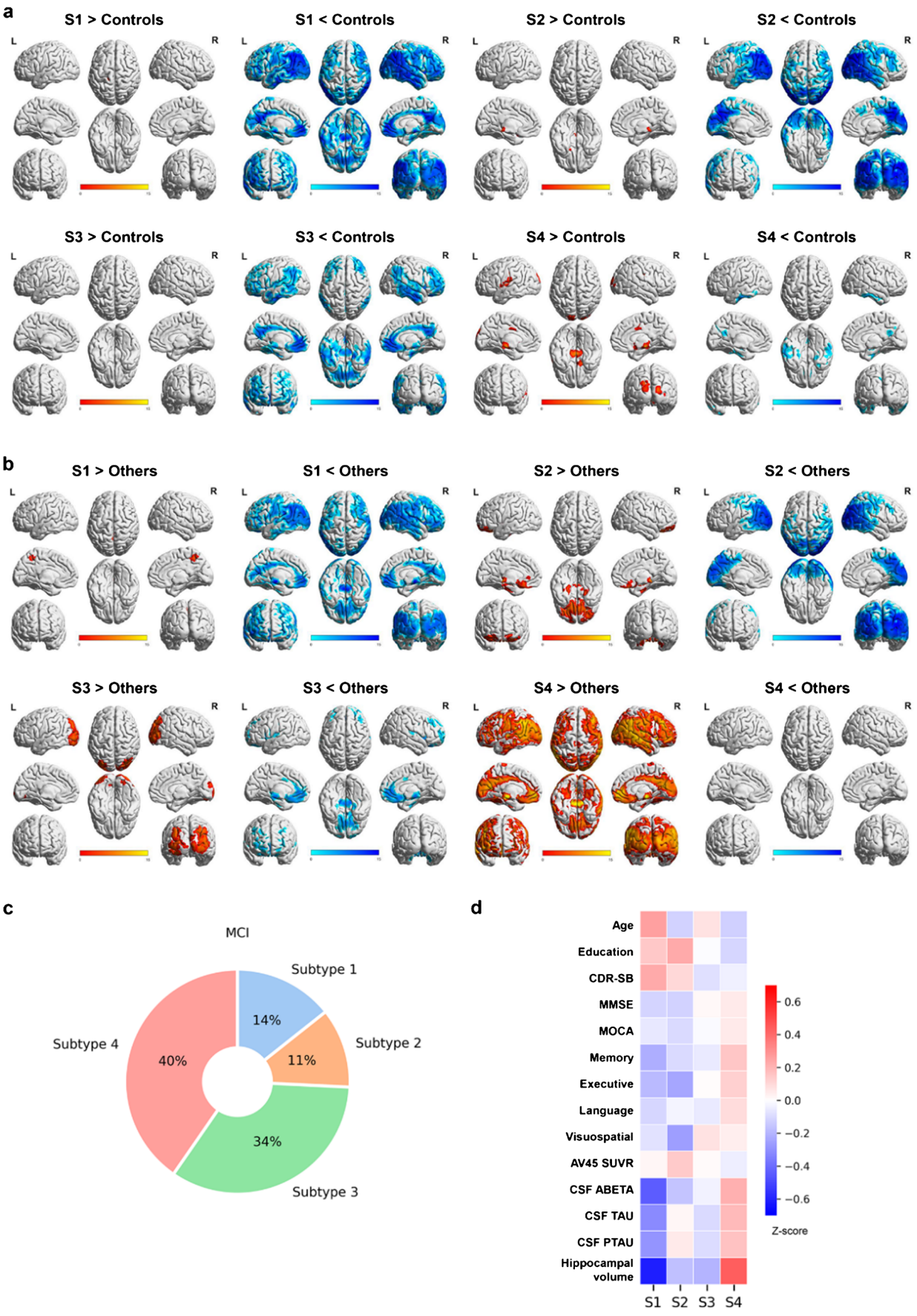
a
S1 > Controls
S1 < Controls
S2 > Controls
S2 < Controls
S3 > Controls
S3 < Controls
S4 > Controls
S4 < Controls
b
S1 > Others
S1 < Others
S2 > Others
S2 < Others
S3 > Others
S3 < Others
S4 > Others
S4 < Others
c
MCI
Subtype 1
14%
Subtype 2
11%
Subtype 3
34%
Subtype 4
40%
d
Age
Education
CDR-SB
MMSE
MOCA
Memory
Executive
Language
Visuospatial
AV45 SUVR
CSF ABETA
CSF TAU
CSF PTAU
Hippocampal volume
S1
S2
S3
S4
0.6
0.4
0.2
0.0
−0.2
−0.4
−0.6
Z-score

◂**Fig. 3** Distinct subtypes of spatial metabolism patterns in MCI. Spatial metabolism patterns of MCI subtypes compared with **a** cognitively normal controls and **b** all other subtypes. The colored bar indicates *t* values. **c** Frequency of MCI subtypes. **d** Heatmap of clinical and biological characteristics of MCI subtypes

(34%), respectively. The subtype-specific hypometabolism patterns observed in AD at the baseline visit resembled those observed in the analysis using all AD images (Supplementary Fig. 4). Subgroup analysis with amyloid-positive AD also showed similar subtype-specific spatial metabolism patterns (Supplementary Fig. 5a-b).

We attempted to check whether the subtype persisted in the case of longitudinal follow-up PET images. The distances between centroids and individuals in each subtype showed a stable trend without dramatic changes, implying that the subtypes were stable during longitudinal follow-up (Supplementary Fig. 6).

Clinical and biological characterization of AD subtypes

CDR-SB scores did not show a significant difference across AD subtypes (Table 1, Supplementary Table 2 and 3). Compared to other subtypes, S1 (angular) included the highest frequencies of males and more educated individuals. Individuals in S1 showed less CSF Abeta and higher SUVR of AV45 PET, but lower CSF p-tau and t-tau levels. S1 individuals tended to have smaller hippocampal volumes. S2 (occipital) individuals were younger and had more overall tau burden but less hippocampal atrophy. S2 individuals tended to have better relative memory and language scores but worse relative executive and visuospatial scores. S3 (orbitofrontal) individuals were older and had less amyloid burden but more hippocampal atrophy. S3 individuals tended to have better executive and visuospatial scores. Finally, S4 (minimal) included the highest frequencies of females and less educated individuals. S4 individuals had more tau burden but less hippocampal atrophy. S4 individuals tended to have better executive, language, and visuospatial scores (Fig. 2c–e, Table 1). Subgroup analysis with amyloid-positive AD also showed similar patterns of clinical and biological characteristics across the subtypes (Supplementary Fig. 5c-d, Supplementary Table 4).

Applying the model to classify MCI subjects

The trained model in AD was transferred to the MCI images for subtyping MCI. Spatial brain metabolism patterns with cerebellar normalization of MCI subtypes (MCI-S) were compared with those of the CN (Fig. 3a). MCI-S1, MCI-S2, and MCI-S3 shared a typical AD pattern of hypometabolism involving the frontal, parietal, and temporal lobes, precuneus, and posterior cingulate cortex. Unlike S4 in AD, MCI-S4 showed a minimal region of hypometabolism compared to CN. In addition to the shared pattern of hypometabolism, subtype-specific spatial metabolism patterns in MCI resembled those observed in AD. As shown in AD subtypes, MCI-S1 (angular) showed prominent hypometabolism in the angular gyrus with a diffuse hypometabolism pattern. MCI-S2 (occipital) showed prominent hypometabolism in the occipital cortex with a posterior-predominant hypometabolism pattern, and MCI-S3 (orbitofrontal) showed prominent hypometabolism in the orbitofrontal cortex with an anterior-predominant hypometabolism pattern. MCI-S4 (minimal) did not show additional subtype-specific regions of hypometabolism. Subtype-specific spatial metabolism patterns in MCI also corresponded to the regions observed in the comparisons between one subtype and all of the other subtypes (Fig. 3b). Different from the distribution of subtypes in AD, individuals in the MCI group were less distributed in S1 and S2 but more distributed in S3 and S4: the numbers in S1, S2, S3, and S4 were 252 (14%), 202 (11%), 596 (34%), and 711 (40%), respectively (Fig. 3c).

CDR-SB scores were significantly different across the MCI subtypes ($P < 0.001$); CDR-SB scores were the highest in MCI-S1 but the lowest in MCI-S3. MCI-S1 included the highest frequency of males, and the individuals in MCI-S1 had more amyloid burden and more hippocampal atrophy but less overall tau burden, which was a similar pattern observed in AD subtypes. In addition, individuals in MCI-S1 tended to have lower memory, executive, language, and visuospatial scores. Individuals in MCI-S2 were younger than those in other subtypes. MCI-S2 tended to have more overall tau burden and better language but worse executive and visuospatial scores, as similarly observed in S2 of AD. Individuals in MCI-S3 tended to have a less amyloid burden and higher executive and visuospatial scores, as observed in S3 of AD. Finally, MCI-S4 included the highest frequencies of females and less educated individuals, as observed in S4 of AD. Individuals in MCI-S4 had the most favorable clinical presentation: higher MOCA, MMSE, memory, executive, language, and visuospatial scores. MCI-S4 had the lowest amyloid deposits and less hippocampal atrophy among the subtypes but had more tau burden (Fig. 3d and Supplementary Table 5).

Prognosis prediction of subtypes for conversion from MCI to AD

There was a significant difference in the frequency of MCI to AD conversion within a 2-year follow-up across the subtypes ($P < 0.001$). MCI to AD conversion was observed more frequently in S1 (23.4%, 18/77) and S2 (35.7%, 25/70) than in S3 (16.7%, 35/210) and S4 (12.7%, 31/245) (Fig. 4a). Individuals in S2 also had a significantly faster conversion

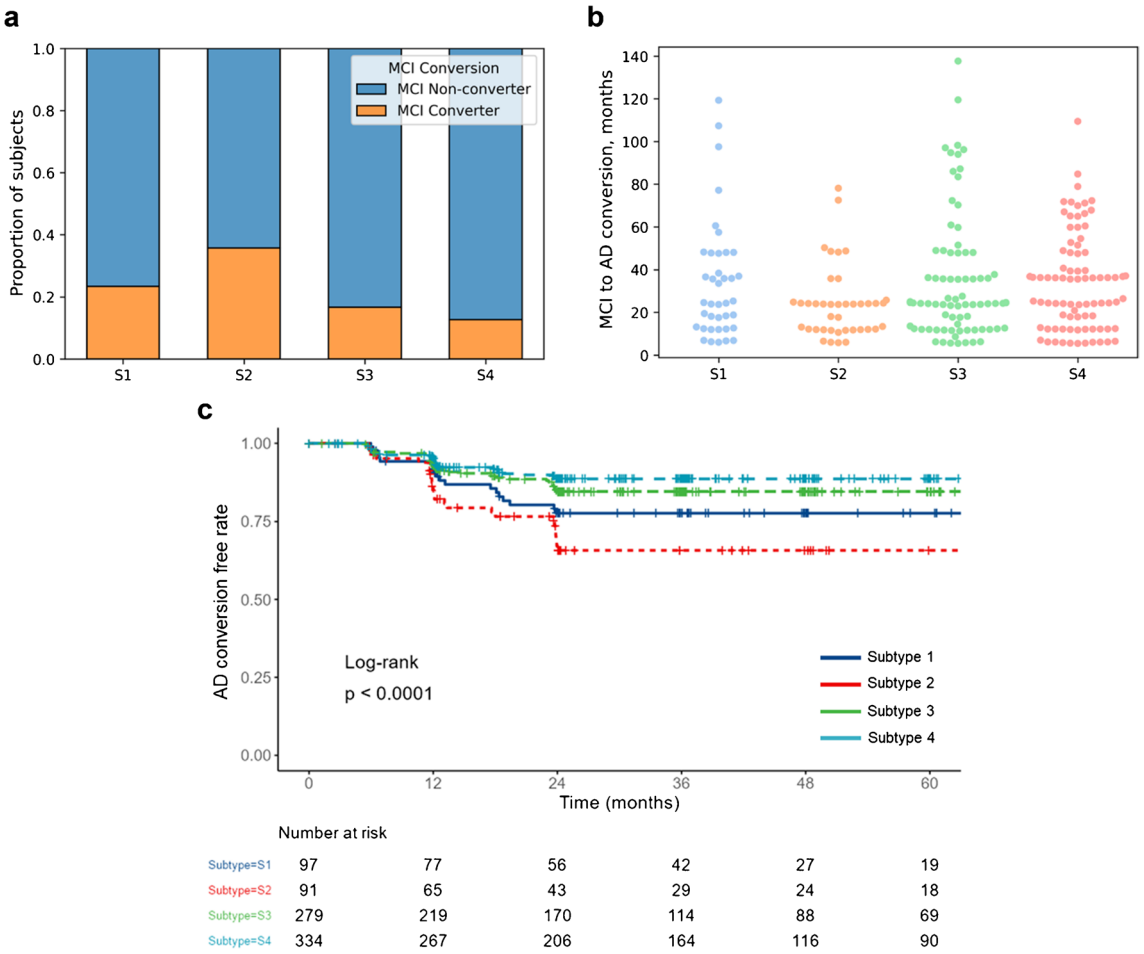

Fig. 4 Prognosis of subtypes for conversion from MCI to AD. **a** Frequency of MCI converters across subtypes. The *y*-axis shows the percentage of MCI converters and non-converters in each subtype. **b** Time to conversion from MCI to AD. The *y*-axis shows the months for the conversion from MCI to AD in each subtype. **c** Kaplan-Meier survival curve for the conversion from MCI to AD across subtypes

from MCI to AD (S2 vs. S3, 24.0 vs. 35.3 months, $P = 0.047$; S2 vs. S4, 24.0 vs. 34.0 months, $P = 0.037$; Fig. 4b and Supplementary Table 6). There was a significant difference in the risk of conversion across the subtypes (log-rank $P < 0.0001$). S2 showed the highest risk of conversion from MCI to AD, followed by S1 (Fig. 4c).

Discussion

In this study, we identified distinct subtypes of spatial brain metabolism patterns in AD with different clinicopathologic features using deep learning-based FDG PET clusters (summarized in Fig. 5). Our deep learning model was also successfully transferred to predict the prognosis of subtypes for conversion from MCI to AD.

Our results suggest that the deep learning model could predict the distinct subtype of brain metabolism patterns in AD, independent of disease progression. The hypothesis-driven approach to neuroimaging might not provide a comprehensive description and cannot reflect heterogeneous clinicopathologic profiles of AD since the study design was limited to the prior definition of neuropathologic subtypes. The unsupervised approach could help to make new discoveries of unappreciated subtypes, and it is expected to overcome the limitations of prior definitions in hypothesis-driven studies. Above all, the key contribution of our study is the application of the cVAE model, which has a structure of additional input information for the condition of each image [21, 30]. When we provided AD severity information (CDR-SB) as an input condition of FDG PET images in the cVAE model, the latent space could reflect hidden heterogeneity information about AD other than disease severity. When cVAE with the CDR-SB condition was applied, there were no significant differences in CDR-SB across the AD subtypes ($P = 0.609$), and the brain metabolism pattern showed distinct features with different clinicopathologic profiles. The considerable disagreement in subtypes between

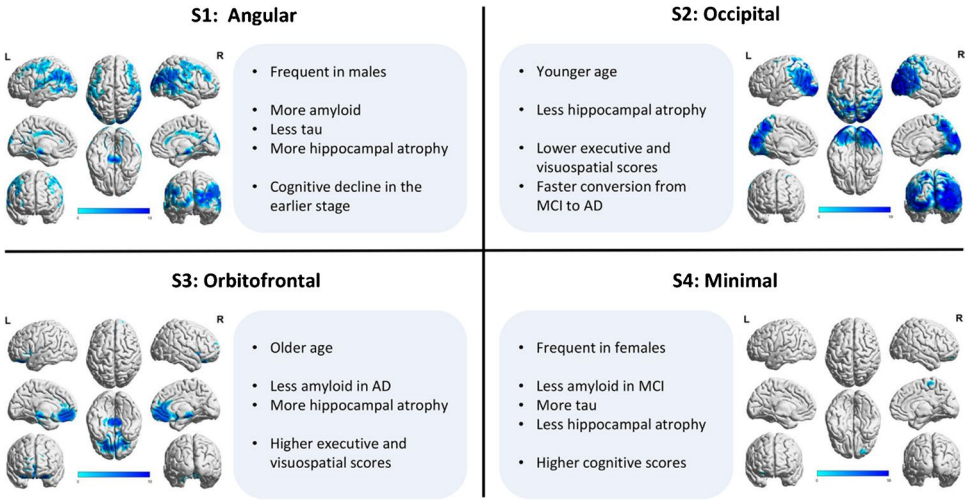

Fig. 5 Summarizing subtypes of spatial metabolism patterns in AD and MCI. Four distinct subtypes of spatial metabolism patterns with different brain pathologies and clinical profiles were identified. The text in bold indicates subtype-specific hypometabolic regions from each subtype (colored blue in the brain). The text in the box indicates the clinical and biological characteristics of each subtype

previous reports and the current study is likely due to the presence or absence of severity dimensions, along with the AD subtypes.

In this study, we could predict the prognosis of the AD subtype by transferring our deep learning model for subtyping MCI. Biomarkers for the early detection of MCI conversion and prediction of prognosis and disease course are important to submit patients to early treatment before the staging of AD. There have been many previous studies on the development of biomarkers and models to predict MCI to AD conversion [31–33]. In the clinic, it is even more difficult to differentiate biological subtypes and predict the prognosis of individual AD and MCI patients since the symptoms and clinical characteristics are diverse and complex. In our study, the predicted MCI subtypes by transferring the trained model revealed significantly different prognoses for MCI to AD conversion. The spatial metabolism patterns and the clinical profiles in MCI subtypes were similar but with some differences from those in AD. These findings imply that subtypes might have distinct trajectories of disease progression with different features in earlier and late stages. Moreover, the heterogeneity of MCI subjects, which included patients originating from other disease populations who were not associated with the progression of amyloid pathology, affects the differences in the subtyping of MCI. Recent studies have revealed that the AD-derived subtype patterns in MCI, clustered based on the patterns observed in AD, exhibited distinct biological and clinical characteristics with a different risk of progression to AD, which aligns with the findings in our study [15, 34, 35]. MCI is a heterogeneous group, which may include subjects without AD-related pathophysiology, representing a potential limitation of this approach. However, FDG PET can offer functional brain patterns that are associated with clinical symptoms and reflect the continuous symptomatic spectrum of AD. Consequently, we applied our clustering patterns to MCI patients. While distinct subtypes might ultimately converge into a common pattern in the later stages of the disease, using deep learning-based models to predict outcomes in AD and MCI subtypes with FDG PET has significant clinical implications. This approach can potentially aid in individualized diagnosis and early intervention, which could inform future treatment strategies for AD.

The subtypes of AD based on FDG PET have added value as a predictive biomarker compared to other biomarkers as well as revealing the heterogeneity of AD. An advantage of FDG PET over amyloid PET is its ability to predict clinical stability or progression of cognitive decline. This is evidenced by the fact that amyloid-positive subjects without hypometabolic abnormalities have remained clinically stable over time [36]. The APOE4, which is the strongest genetic risk factor for AD, also presents limitations as biomarkers reflecting the heterogeneity of MCI and AD, as atypical phenotypes are less likely to carry APOE4 compared to those with typical presentations [37–39]. We are not simply trying to show that FDG PET-based subtypes are better prognostic markers than other biomarkers. The important idea behind our findings is that AD is heterogeneous, that FDG PET can indicate subtypes, and that these subtypes may be meaningful because other biomarkers and prognoses differ across subtypes. The heterogeneity of AD might be linked to complex biological processes including amyloid-tau-neurodegeneration (A/T/N) and various genetic, cellular, or network abnormalities. Thus, our distinct subtypes of FDG will serve as a powerful tool that can be used in combination with other biomarkers.

In the clinical setting, differentiating subtype-specific metabolism patterns on FDG PET only with visual interpretation is very difficult and subject to interobserver

variability. Because of diffuse overlapping regions of hypometabolism (typical AD pattern) across the subtypes, it is difficult to distinguish subtype-specific hypometabolic regions only with visual interpretation, as shown in our generated images (Supplementary Fig. 7) and statistical parametric maps of FDG PET with cerebellar normalization. It could also be extended to the form of artificial intelligence-empowered imaging biomarkers, which could provide new information based on deep learning beyond visual interpretation.

Some limitations should be noted. First, the deep learning model should be further validated by AD datasets, although the ADNI database was large and obtained from multiple centers. Second, the deep learning model trained in the AD group was directly transferred to the MCI group. However, MCI is a heterogeneous syndrome resulting from AD, as well as non-AD and non-neurodegenerative conditions [40–43], implying that some of the patients in our MCI group might have originated from other disease populations different from AD. Finally, a larger longitudinal study might be warranted to investigate the subtype-specific trajectory of spatial metabolism changes and clinicopathologic profiles.

Conclusion

In this study, we identified distinct subtypes in AD with different brain pathologies and clinical profiles. Additionally, our model was successfully transferred to predict the prognosis of subtypes for conversion from MCI to AD. Our results suggest that distinct AD subtypes on FDG PET could have implications for individual clinical outcomes and provide a clue to understanding a broad spectrum of AD in terms of pathophysiology.

Supplementary Information The online version contains supplementary material available at https://doi.org/10.1007/s00259-023-06440-9.

Acknowledgements This paper is based on the first author's Ph.D. thesis in the Graduate School of Convergence Science and Technology, and College of Medicine or College of Pharmacy, Seoul National University, Seoul, Republic of Korea.

Author contribution H.C. designed the study. H.G.R. and H.C. developed the model. H.G.R. performed experiments. A.R. and D.S.L. contributed to analyze PET images. D.Y.L. and D.S.L. contributed to analyze clinical data. K.S. supported developing the model. K.S., A.R., D.Y.L., and D.S.L. contributed to data interpretation and analysis. H.G.R. wrote the manuscript mainly and all authors critically reviewed and edited the manuscript.

Funding This research was supported by the National Research Foundation of Korea grant funded by the Korea Government (NRF-2019K1A3A1A14065446), and Korea Medical Device Development Fund grant funded by the Korea government (the Ministry of Science and ICT, the Ministry of Trade, Industry and Energy, the Ministry of Health & Welfare, the Ministry of Food and Drug Safety) (Project Number: 1711137868, RS-2020-KD000006).

Data collection and sharing for this project was funded by the Alzheimer's Disease Neuroimaging Initiative (ADNI) (National Institutes of Health Grant U01 AG024904) and DOD ADNI (Department of Defense award number W81XWH-12-2-0012). ADNI is funded by the National Institute on Aging, the National Institute of Biomedical Imaging and Bioengineering, and through generous contributions from the following: AbbVie, Alzheimer's Association; Alzheimer's Drug Discovery Foundation; Araclon Biotech; BioClinica, Inc.; Biogen; Bristol-Myers Squibb Company; CereSpir, Inc.; Cogstate; Eisai Inc.; Elan Pharmaceuticals, Inc.; Eli Lilly and Company; EuroImmun; F. Hoffmann-La Roche Ltd and its affiliated company Genentech, Inc.; Fujirebio; GE Healthcare; IXICO Ltd.; Janssen Alzheimer Immunotherapy Research & Development, LLC.; Johnson & Johnson Pharmaceutical Research & Development LLC.; Lumosity; Lundbeck; Merck & Co., Inc.; Meso Scale Diagnostics, LLC.; NeuroRx Research; Neurotrack Technologies; Novartis Pharmaceuticals Corporation; Pfizer Inc.; Piramal Imaging; Servier; Takeda Pharmaceutical Company; and Transition Therapeutics. The Canadian Institutes of Health Research is providing funds to support ADNI clinical sites in Canada. Private sector contributions are facilitated by the Foundation for the National Institutes of Health (www.fnih.org). The grantee organization is the Northern California Institute for Research and Education, and the study is coordinated by the Alzheimer's Therapeutic Research Institute at the University of Southern California. ADNI data are disseminated by the Laboratory for Neuro Imaging at the University of Southern California.

Data availability All raw data including FDG PET, CDR-SB score, demographic, cognitive, and biomarker variables are available through the ADNI data archive (http://adni.loni.usc.edu/). The custom codes for the deep learning model may be available for research purposes from the corresponding authors on reasonable request.

Declarations

Ethics approval All procedures performed in studies involving human participants were in accordance with the ethical standards of the institutional and/or national research committee and with the 1964 Helsinki Declaration and its later amendments or comparable ethical standards.

Informed consent Written informed consent for cognitive testing and neuroimaging prior to participation of the ADNI cohort was obtained from all subjects, and the study protocols were approved by the institutional review boards of all participating institutions.

Competing interests Dr. Choi is a co-founder of Portrai, Inc. All other authors declare no competing interests.

References

1. Lam B, Masellis M, Freedman M, Stuss DT, Black SE. Clinical, imaging, and pathological heterogeneity of the Alzheimer's disease syndrome. Alzheimers Res Ther. 2013;5:1. https://doi.org/10.1186/alzrt155.
2. Friedland RP, Koss E, Haxby JV, Grady CL, Luxenberg J, Schapiro MB, et al. NIH conference. Alzheimer disease: clinical and biological heterogeneity. Ann Intern Med. 1988;109:298–311. https://doi.org/10.7326/0003-4819-109-4-298.
3. Noh Y, Jeon S, Lee JM, Seo SW, Kim GH, Cho H, et al. Anatomical heterogeneity of Alzheimer disease: based on cortical

thickness on MRIs. Neurology. 2014;83:1936–44. https://doi.org/10.1212/WNL.0000000000001003.
4. Dujardin S, Commins C, Lathuiliere A, Beerepoot P, Fernandes AR, Kamath TV, et al. Tau molecular diversity contributes to clinical heterogeneity in Alzheimer's disease. Nat Med. 2020;26:1256–63. https://doi.org/10.1038/s41591-020-0938-9.
5. Ferreira D, Nordberg A, Westman E. Biological subtypes of Alzheimer disease: a systematic review and meta-analysis. Neurology. 2020;94:436–48. https://doi.org/10.1212/wnl.0000000000009058.
6. Vogel JW, Young AL, Oxtoby NP, Smith R, Ossenkoppele R, Strandberg OT, et al. Four distinct trajectories of tau deposition identified in Alzheimer's disease. Nat Med. 2021;27:871–81. https://doi.org/10.1038/s41591-021-01309-6.
7. Ferreira D, Verhagen C, Hernández-Cabrera JA, Cavallin L, Guo C-J, Ekman U, et al. Distinct subtypes of Alzheimer's disease based on patterns of brain atrophy: longitudinal trajectories and clinical applications. Sci Rep. 2017;7:1–13. https://doi.org/10.1038/srep46263.
8. Mosconi L, Tsui WH, Herholz K, Pupi A, Drzezga A, Lucignani G, et al. Multicenter standardized 18F-FDG PET diagnosis of mild cognitive impairment, Alzheimer's disease, and other dementias. J Nucl Med. 2008;49:390–8. https://doi.org/10.2967/jnumed.107.045385.
9. Meyer PT, Frings L, Rücker G, Hellwig S. 18F-FDG PET in parkinsonism: differential diagnosis and evaluation of cognitive impairment. J Nucl Med. 2017;58:1888–98. https://doi.org/10.2967/jnumed.116.186403.
10. Herholz K, Westwood S, Haense C, Dunn G. Evaluation of a calibrated 18F-FDG PET score as a biomarker for progression in Alzheimer disease and mild cognitive impairment. J Nucl Med. 2011;52:1218–26. https://doi.org/10.2967/jnumed.111.090902.
11. Landau S, Harvey D, Madison C, Reiman E, Foster N, Aisen P, et al. Comparing predictors of conversion and decline in mild cognitive impairment. Neurology. 2010;75:230–8. https://doi.org/10.1212/WNL.0b013e3181e8e8b8.
12. Besson FL, La Joie R, Doeuvre L, Gaubert M, Mézenge F, Egret S, et al. Cognitive and brain profiles associated with current neuroimaging biomarkers of preclinical Alzheimer's disease. J Neurosci. 2015;35:10402–11. https://doi.org/10.1523/JNEUROSCI.0150-15.2015.
13. Laforce R Jr, Soucy J-P, Sellami L, Dallaire-Théroux C, Brunet F, Bergeron D, et al. Molecular imaging in dementia: past, present, and future. Alzheimers Dement. 2018;14:1522–52. https://doi.org/10.1016/j.jalz.2018.06.2855.
14. Vanhoutte M, Semah F, Sillaire AR, Jaillard A, Petyt G, Kuchcinski G, et al. 18F-FDG PET hypometabolism patterns reflect clinical heterogeneity in sporadic forms of early-onset Alzheimer's disease. Neurobiol Aging. 2017;59:184–96. https://doi.org/10.1016/j.neurobiolaging.2017.08.009.
15. Levin F, Ferreira D, Lange C, Dyrba M, Westman E, Buchert R, et al. Data-driven FDG-PET subtypes of Alzheimer's disease-related neurodegeneration. Alzheimers Res Ther. 2021;13:49. https://doi.org/10.1186/s13195-021-00785-9.
16. Groot C, Risacher SL, Chen JQA, Dicks E, Saykin AJ, Mac Donald CL, et al. Differential trajectories of hypometabolism across cognitively-defined Alzheimer's disease subgroups. Neuroimage Clin. 2021;31:102725. https://doi.org/10.1016/j.nicl.2021.102725.
17. Jo T, Nho K, Saykin AJ. Deep learning in Alzheimer's disease: diagnostic classification and prognostic prediction using neuroimaging data. Front Aging Neurosci. 2019;11:220. https://doi.org/10.3389/fnagi.2019.00220.
18. Zhao Z, Chuah JH, Lai KW, Chow CO, Gochoo M, Dhanalakshmi S, et al. Conventional machine learning and deep learning in Alzheimer's disease diagnosis using neuroimaging: a review. Front Comput Neurosci. 2023;17:1038636. https://doi.org/10.3389/fncom.2023.1038636.
19. Young AL, Marinescu RV, Oxtoby NP, Bocchetta M, Yong K, Firth NC, et al. Uncovering the heterogeneity and temporal complexity of neurodegenerative diseases with subtype and stage inference. Nat Commun. 2018;9:4273. https://doi.org/10.1038/s41467-018-05892-0.
20. Kingma DP, Welling M. Auto-encoding variational bayes. arXiv preprint arXiv:1312.6114, 2013.
21. Kingma DP, Mohamed S, Rezende DJ, Welling M. Semi-supervised learning with deep generative models. arXiv preprint arXiv:1406.5298, 2014.
22. Jagust WJ, Landau SM, Koeppe RA, Reiman EM, Chen K, Mathis CA, et al. The Alzheimer's disease neuroimaging initiative 2 PET core: 2015. Alzheimers Dement. 2015;11:757–71. https://doi.org/10.1016/j.jalz.2015.05.001.
23. Hughes CP, Berg L, Danziger W, Coben LA, Martin RL. A new clinical scale for the staging of dementia. Br J Psychiatry. 1982;140:566–72. https://doi.org/10.1192/bjp.140.6.566.
24. Choi H, Kang H, Lee DS. Predicting aging of brain metabolic topography using variational autoencoder. Front Aging Neurosci. 2018;10:212. https://doi.org/10.3389/fnagi.2018.00212.
25. Lloyd S. Least squares quantization in PCM. IEEE Trans Inf Theory. 1982;28:129–37. https://doi.org/10.1109/TIT.1982.1056489.
26. MacQueen J. Some methods for classification and analysis of multivariate observations. Proceedings of the 5th Berkeley symposium on mathematical statistics and probability. 1967:281-97.
27. Kodinariya TM, Makwana PR. Review on determining number of Cluster in K-Means Clustering. Int J Adv Res Comput Sci Manage Stud. 2013;1:90–5.
28. Marutho D, Handaka SH, Wijaya E. The determination of cluster number at k-mean using elbow method and purity evaluation on headline news. Proceedings of the 2018 International Seminar on Application for Technology of Information and Communication. 2018:533-8.
29. Mukherjee S, Choi SE, Lee ML, Scollard P, Trittschuh EH, Mez J, et al. Cognitive domain harmonization and cocalibration in studies of older adults. Neuropsychology. 2023;37:409–23. https://doi.org/10.1037/neu0000835.
30. Sohn K, Lee H, Yan X. Learning structured output representation using deep conditional generative models. Proceedings of the 28th International Conference on Neural Information Processing Systems. 2015:3483-91.
31. Misra C, Fan Y, Davatzikos C. Baseline and longitudinal patterns of brain atrophy in MCI patients, and their use in prediction of short-term conversion to AD: results from ADNI. Neuroimage. 2009;44:1415–22. https://doi.org/10.1016/j.neuroimage.2008.10.031.
32. Davatzikos C, Bhatt P, Shaw LM, Batmanghelich KN, Trojanowski JQ. Prediction of MCI to AD conversion, via MRI, CSF biomarkers, and pattern classification. Neurobiol Aging. 2011;32:2322.e19-e27. https://doi.org/10.1016/j.neurobiolaging.2010.05.023.
33. Cheng B, Liu M, Zhang D, Munsell BC, Shen D. Domain transfer learning for MCI conversion prediction. IEEE Trans Biomed Eng. 2015;62:1805–17. https://doi.org/10.1109/TBME.2015.2404809.
34. Kwak K, Giovanello KS, Bozoki A, Styner M, Dayan E. Subtyping of mild cognitive impairment using a deep learning model based on brain atrophy patterns. Cell Rep Med. 2021;2:100467. https://doi.org/10.1016/j.xcrm.2021.100467.
35. Chen P, Yao H, Tijms BM, Wang P, Wang D, Song C, et al. Four distinct subtypes of Alzheimer's disease based on resting-state connectivity biomarkers. Biol Psychiatry. 2023;93:759–69. https://doi.org/10.1016/j.biopsych.2022.06.019.
36. Iaccarino L, Sala A, Perani D. Predicting long-term clinical stability in amyloid-positive subjects by FDG-PET. Ann Clin Transl Neurol. 2019;6:1113–20. https://doi.org/10.1002/acn3.782.
37. van der Flier WM, Pijnenburg YA, Fox NC, Scheltens P. Early-onset versus late-onset Alzheimer's disease: the case of the

missing APOE ε4 allele. Lancet Neurol. 2011;10:280–8. https://doi.org/10.1016/s1474-4422(10)70306-9.
38. Rogalski E, Sridhar J, Rader B, Martersteck A, Chen K, Cobia D, et al. Aphasic variant of Alzheimer disease: clinical, anatomic, and genetic features. Neurology. 2016;87:1337–43. https://doi.org/10.1212/wnl.0000000000003165.
39. Schott JM, Crutch SJ, Carrasquillo MM, Uphill J, Shakespeare TJ, Ryan NS, et al. Genetic risk factors for the posterior cortical atrophy variant of Alzheimer's disease. Alzheimers Dement. 2016;12:862–71. https://doi.org/10.1016/j.jalz.2016.01.010.
40. Petersen RC. Mild cognitive impairment as a diagnostic entity. J Intern Med. 2004;256:183–94. https://doi.org/10.1111/j.1365-2796.2004.01388.x.
41. Jack CR Jr, Knopman DS, Weigand SD, Wiste HJ, Vemuri P, Lowe V, et al. An operational approach to National Institute on Aging-Alzheimer's Association criteria for preclinical Alzheimer disease. Ann Neurol. 2012;71:765–75. https://doi.org/10.1002/ana.22628.
42. Wisse LEM, Butala N, Das SR, Davatzikos C, Dickerson BC, Vaishnavi SN, et al. Suspected non-AD pathology in mild cognitive impairment. Neurobiol Aging. 2015;36:3152–62. https://doi.org/10.1016/j.neurobiolaging.2015.08.029.
43. Jack CR Jr, Knopman DS, Chételat G, Dickson D, Fagan AM, Frisoni GB, et al. Suspected non-Alzheimer disease pathophysiology–concept and controversy. Nat Rev Neurol. 2016;12:117–24. https://doi.org/10.1038/nrneurol.2015.251.